Correction of ocular and atmospheric wavefronts: a comparison of the performance of various deformable mirrors

Nicholas Devaney,* Eugenie Dalimier, Thomas Farrell, Derek Coburn, Ruth Mackey, David Mackey, Francois Laurent, Elizabeth Daly, and Chris Dainty

School of Experimental Physics, National University of Ireland, Galway, Ireland

*Corresponding author: nicholas.devaney@nuigalway.ie

Received 6 June 2008; revised 15 September 2008; accepted 5 November 2008; posted 6 November 2008 (Doc. ID 97121); published 4 December 2008

The main applications of adaptive optics are the correction of the effects of atmospheric turbulence on ground-based telescopes and the correction of ocular aberrations in retinal imaging and visual simulation. The requirements for the wavefront corrector, usually a deformable mirror, will depend on the statistics of the aberrations to be corrected; here we compare the spatial statistics of wavefront aberrations expected in these two applications. We also use measured influence functions and numerical simulations to compare the performance of eight commercially available deformable mirrors for these tasks. The performance is studied as a function of the size of the optical pupil relative to the actuated area of the mirrors and as a function of the number of modes corrected. In the ocular case it is found that, with the exception of segmented mirrors, the performance is greatly enhanced by having a ring of actuators outside the optical pupil, as this improves the correction of the pupil edge. The effect is much smaller in the case of Kolmogorov wavefronts. It is also found that a high Strehl ratio can be obtained in the ocular case with a relatively low number of actuators if the stroke is sufficient. Increasing the number of actuators has more importance in the Kolmogorov case, even for the relatively weak turbulence considered here.

OCIS codes: 110.1080, 330.4460, 230.3990.

1. Introduction

Adaptive optics (AO) was originally proposed in the 1950s by Babcock and, independently, by Linnik as a way to correct for the effects of atmospheric turbulence in astronomical imaging [1,2]. It was first demonstrated in the contexts of astronomical imaging [3] and satellite imaging (see Hardy [4] for a summary of the early history of AO). In the late 1980s, Dreher *et al.* [5] used a deformable mirror to correct prescription astigmatism in a laser tomographic scanner and AO has since been incorporated into different types of retinal imagers, including fundus cameras [6], scanning laser ophthalmoscopes [7,8] and optical coherence tomographs [9,10]. The possibility of using AO to study the effects of ocular aberrations on visual performance has also been investigated [11–15]. When Liang *et al.* [16] first demonstrated the closed-loop correction of ocular aberrations, they used a deformable mirror developed for use in astronomy. However, an obvious difference between astronomical and ocular AO is that the size of the pupil of the system to be corrected is orders of magnitude different. It therefore makes sense to use much smaller deformable mirrors for ocular AO. This also has the advantage of requiring shorter focal lengths, and so the system can be more compact. The development of micromachined mirrors opened up the possibility of using cheap, commercially available deformable mirrors in ocular AO systems, and one could envisage widespread deployment of AO-corrected retinal imaging systems. The first, cheap deformable mirrors were membrane

0003-6935/08/356550-13$15.00/0

micromachined deformable mirrors (MMDM) developed by Flexible BV (formerly OKO Technologies). Fernández and Artal [17] were the first to study their performance in an ocular AO system. A disadvantage of this type of mirror is that it is difficult to correct high spatial frequency phase errors due to the large size of the actuator influence functions. An alternative approach is microelectromechanical systems (MEMS) mirrors which can have a very large number of actuators having relatively localized influence functions. Boston Micromachines has commercialized MEMS mirrors, with models having 32, 140, and 1024 actuators. They are developing a 4096 actuator device for high-contrast astronomical imaging [18]. Doble *et al.* [19] demonstrated the use of the 140 actuator device and achieved performance comparable to that obtained with a conventional Xinetics deformable mirror (DM), which was developed for use in astronomy. Another type of commercial MEMs mirror is the segmented mirror available from Iris AO [20].

Other types of deformable mirror have become commercially available and have been tested in ocular AO systems. These include bimorph mirrors [21] and magnetic deformable mirrors [22], both of which were originally developed for astronomical AO.

Here we present the result of a study of eight different commercially available deformable mirrors, including most of the mirrors mentioned above. We predict their performance for correction of both ocular aberrations and aberrations caused by atmospheric turbulence based on their measured influence functions. Where appropriate, we optimize performance by varying the size of the optical pupil on the mirrors and by selecting the number of mirror modes to correct. Since it is believed that the temporal fluctuations of ocular aberrations are much slower than atmospheric fluctuations, we will concentrate on spatial statistics. This work follows from previous work [23] and studies where we compared the performance of a smaller sample of mirrors [24–26].

The paper is organized as follows. In Section 2 we compare the spatial statistics of wavefronts aberrated by Kolmogorov turbulence and aberrated according to a statistical model of ocular aberrations. In Section 3 we present the mirrors we have studied and summarize the analysis technique. We present comparative results for the correction of ocular aberrations in Section 4 and turbulence-induced aberrations in Section 5. We finish with a discussion and conclusions.

2. Statistical Models of the Wavefront Aberrations

The atmosphere is a turbulent medium and there are well-developed models for the statistics of the aberrations of light passing through it. Surprisingly, the effect of the eye on light passing through it is less well understood and, although there are models relating the familiar ocular, low-order aberrations to anatomical structure (see [27,28] and references therein), there is no model to predict the statistics of ocular aberrations across a population of either healthy or diseased eyes. Here we review what the standard model of atmospheric turbulence tells us about the wavefront aberrations and what can be inferred from ocular models based on measurements.

A. Kolmogorov Model for Atmospheric Aberrations

It has long been known that atmospheric turbulence limits the spatial resolution which can be obtained with ground-based telescopes. Kolmogorov developed a theory of turbulence in the 1940s and this was incorporated into a theory of propagation though turbulence by Tatarski in the 1950s (see Roddier [29] for a classic monograph on the optical effects of turbulence). Fried introduced the concept of a coherence parameter, r_0, over which the root-mean-square (rms) phase fluctuation of a wavefront is 1 rad [30]. For atmospheric turbulence, this parameter depends on the turbulence strength integrated along the optical path and on wavelength ($r_0 \propto \lambda^{6/5}$). The turbulence is concentrated in different regions, notably near the ground and at the tropopause, and it usually occurs in thin layers. Movement of the layers gives rise to dynamic turbulence. According to the "Taylor hypothesis," the turbulence moves as a frozen screen with a speed v and the timescale for evolution of the turbulence-aberrated wavefronts is given by $\tau \approx 0.3 r_0/v$ [31]. The statistics of the turbulence-induced aberrations are normally assumed to be stationary in space and time.

Noll [32] calculated the statistics of a decomposition of turbulence-induced wavefront errors onto the basis set of Zernike polynomials. This set of polynomials is orthogonal on the unit circle and is frequently used to describe aberrations [33]. The polynomials are defined by their radial order n and azimuthal frequency m and we order the polynomials according to the ANSI standards [34].

If the wavefront decomposition is defined by

$$\phi(\mathbf{r}) = \sum_i a_i Z_i(\mathbf{r}), \tag{1}$$

where Z_i are the Zernike modes, then the covariance of the modes has the form

$$\langle a_i a_j \rangle = c_{ij} (D/r_0)^{5/3}, \tag{2}$$

where D is the pupil diameter. Noll published an analytical expression for the coefficients, c_{ij}. The covariance matrix is not diagonal and relatively strong correlations are found between tip and tilt and corresponding coma terms, and between defocus and spherical aberration. Wang and Markey [35] and later Dai [36] extended the analysis to a decomposition on Karhunen–Loève functions, which are statistically independent. These analyses allow the residual wavefront error to be calculated as a function of the number of Zernike (or Karhonen–Loève) modes corrected by an AO system. From Eq. (2) it can be seen that the residual variance when N modes are corrected is given by

$$\sigma^2 = \alpha_N (D/r_0)^{5/3}. \quad (3)$$

This relation can be used to determine how many modes should be corrected in order to achieve a given wavefront residual and, hence, image quality. As an alternative to this modal approach to wavefront correction, a zonal approach can be employed to determine the number of actuators required to reduce the wavefront error variance to the required level. In general, it is found [37] that

$$\sigma^2 = \beta (d/r_0)^{5/3}, \quad (4)$$

where d is the actuator spacing. The coefficient β depends on the actuator influence functions, with theoretical values ranging from 0.24 for continuous-plate mirrors with Gaussian influence functions to 1.26 for piston-only segmented mirrors [4].

The residual wavefront variance does not give complete information on the wavefront correction, as the corrected wavefront is nonstationary, i.e., the variance depends on position within the pupil. Conan [38] recently published a study of the residual wavefront variance over the optical pupil as a function of the number of Zernike modes corrected, showing that the variance increases toward the pupil edge. For pure Kolmogorov turbulence, the rms phase at the edge of the pupil is 35% higher than the average over the pupil. This could have an impact on the requirements for deformable mirror stroke, which is usually determined as simply some multiple of the piston and tip–tilt corrected wavefront rms error. There is a high residual at the pupil edge even when a relatively large number of modes are corrected, although the area over which there is residual error decreases as a function of the number of modes corrected.

B. Thibos Model for Ocular Aberrations

Aberrations of the eye will limit the spatial resolution of retinal images for pupil diameters larger than about 2 mm. The aberrations are partially due to errors in the main optical elements of the eye, i.e., the cornea and lens, but is also due to the tear film. While defocus and astigmatism are the largest aberrations, and present the greatest variability between subjects, it is known that higher-order aberrations are also significant: typically, they represent around 10% of the total variance of the wave aberration for a pupil between 5 and 7 mm diameter [39,40]. The aberrations are dynamic and measurements have found fluctuations in the aberrations falling at −4 dB per octave up to at least 70 Hz [41]. It is not clear what the origin of the aberration dynamics is, but possible factors include microfluctuations of accommodation, retinal pulsation, and changes in the tear-film thickness over the cornea.

In contrast to the case of atmospheric turbulence, there is no theory capable of predicting the aberration statistics of ocular wavefronts. In the absence of such a theory, it is common practice to employ statistics determined by measurements on samples of real eyes. The most widely used statistics are those published by Thibos *et al.* [42] based on a study of the 200 normal, healthy eyes. The eyes were corrected subjectively for defocus and astigmatism to the nearest 0.25 diopters (D). The mean residual for defocus over the population is 0.25 D, while that of astigmatism is less than 0.1 D. The measurements were made with a Shack–Hartmann sensor and decomposed onto Zernike polynomials, according to the ANSI standards [34]. Although one might argue against the small sample size and the fact that the aberrations were measured only up to the 7th Zernike order, we will base our analysis of the correction of ocular aberrations on these statistics as being the best available. According to this model, all the aberration coefficients have zero mean, with the exception of spherical aberration, which has a positive bias. This contrasts with atmospheric turbulence, for which the mean of all aberrations is assumed to be zero. Positive correlations are found between tip–tilt and the corresponding coma terms and between defocus and spherical aberration. As Thibos points out, if the eye contains a simple Seidel aberration, such as spherical aberration, then this will lead to Zernike spherical aberration plus correlated defocus. Figure 1 shows a comparison of the variances of the Zernike coefficients of order 2 and higher for Kolmogorov turbulence and the Thibos model for a 6 mm eye. The curves are normalized to each have a total variance of unity. We note in passing that the tip–tilt corrected wavefront rms for a 6 mm pupil eye is 0.68 μm in the Thibos model, which is comparable to the wavefront rms error on an 8 m telescope in good seeing ($r_0 = 18$ cm at 0.5 μm). It appears from Fig. 1 that the high orders fall off faster for the Thibos model than for the Kolmogorov model, with the exception of spherical aberration. This suggests that low-order correction may be more relevant in the case of ocular AO. However, both Thibos and

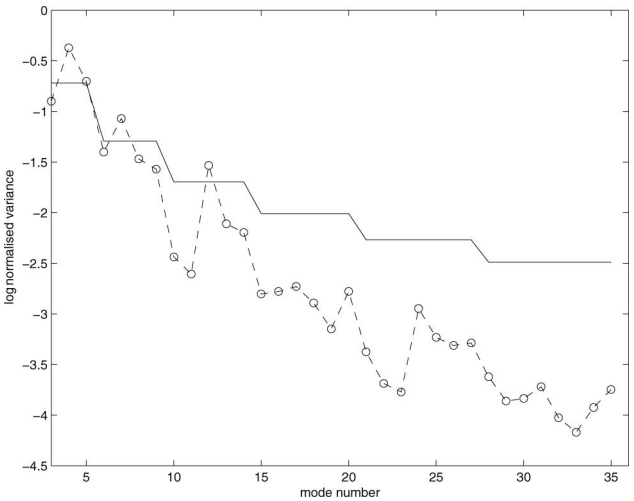

Fig. 1. Zernike coefficients for decomposition of Kolmogorov turbulence (solid curve) and Thibos model 6 mm eye (dashed curve). Both curves are normalized to have a total variance of unity. Mode 12 corresponds to spherical aberration.

Castejón-Mochón *et al.* [40,42] have shown that higher-order aberrations are relatively more important as pupil diameter increases; i.e., the percentage of the total aberration due to aberrations with radial order $n > 2$ increases as the pupil diameter increases. In the same paper, Castejón-Mochón *et al.* find that the rms aberration increases as the square of the ocular diameter, which is faster than the $D^{5/6}$ relation in the case of increasing aperture size in turbulence. Miller *et al.* [43] examined the requirements for segmented correctors in AO retinal imaging with large (>6 mm) ocular pupils using aberration measurements from a sample of 12 normal eyes. They simulated the performance of deformable mirrors with different numbers of actuators and calculated the number of actuators required to give a Strehl ratio of 0.8 as a function of pupil diameter. They found a cubic fit, while the relation would be linear in the case of correcting aberrations due to Kolmogorov turbulence. (Basically, as the aperture increases, the number of actuators increases keeping d/r_0 constant, where d is the actuator spacing.) This shows that a simple fitting error formula, such as Eq. (4), cannot be used to predict the performance of ocular aberration correction as a function of the number of deformable mirror actuators. In general, the number of actuators required to give a certain level of correction will increase faster with pupil size for the case of ocular aberrations than for the case of Kolmogorov turbulence.

We have also examined the wavefront mean and variance over the pupil for wavefronts aberrated according to both the Kolmogorov and Thibos models. We simulated 20,000 ocular wavefronts according to the Thibos model for a pupil diameter of 6 mm and found the mean wavefront and its variance. The results are shown in Figs. 2 and 3. It can be seen that both the mean wavefront and the variance rise from the center of the pupil to the edge. This suggests that the actuator stroke needs to be larger at the edge of the pupil. The rms wavefront error at the pupil edge is approximately seven times higher than at the center, an effect which is much larger than in the case of correcting turbulence.

In addition, we have investigated the nature of the residual wavefront when the first 15 modes are removed. Cagigal *et al.* [44] claimed that when this is carried out, the residual wavefront is stationary (i.e., variance the same over the pupil) and the residual wavefronts have Kolmogorov statistics. It can be seen in Fig. 4 that the assumption of stationarity may be correct in the interior of the pupil (although the residuals are very small, when using the Thibos model), but it is clearly not correct in a narrow zone around the edge of the pupil.

3. Characteristics of the Deformable Mirrors and Analysis Method

We have studied the performance of eight commercially available deformable mirrors:

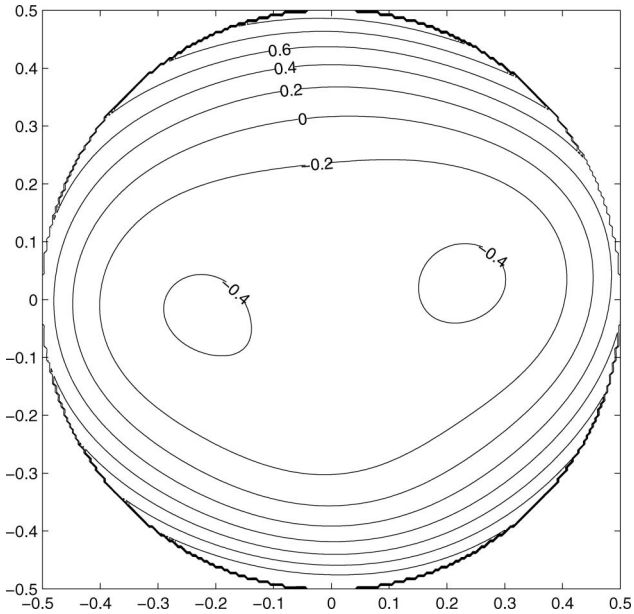

Fig. 2. Wavefront mean for a 6 mm pupil calculated using 20,000 eyes simulated according to the Thibos model with no piston, tip, or tilt. The units are micrometers.

- a 37-channel micromachined membrane deformable mirror (MMDM) from Flexible Optical BV (OKO37) [45],
- a 37-channel MMDM from AgilOptics (AgilOptic37),
- a 37 channel piston/tip/tilt segmented deformable mirror from Iris AO (IrisAO37) [20],
- a 19-channel piezoelectric mirror from Flexible Optical BV (OKO19_PZT),
- a 37-channel piezoelectric mirror from Flexible Optical BV (OKO37_PZT),

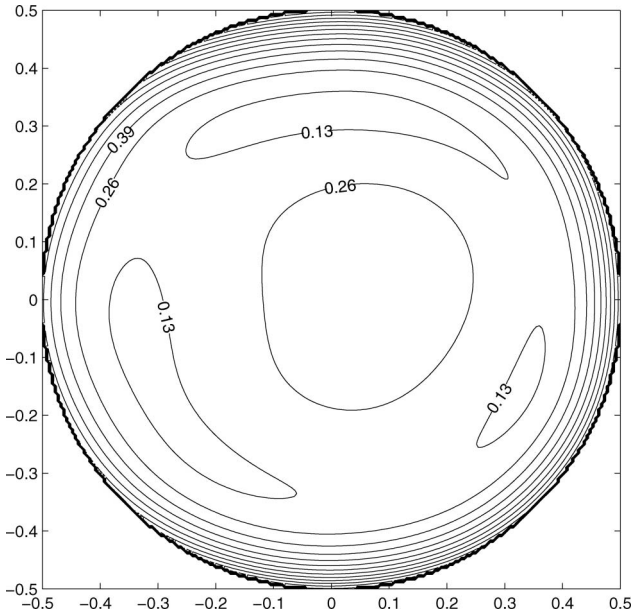

Fig. 3. Wavefront variance for a 6 mm pupil calculated using 20,000 eyes simulated according to the Thibos model with no piston, tip, or tilt. The units are micrometers squared.

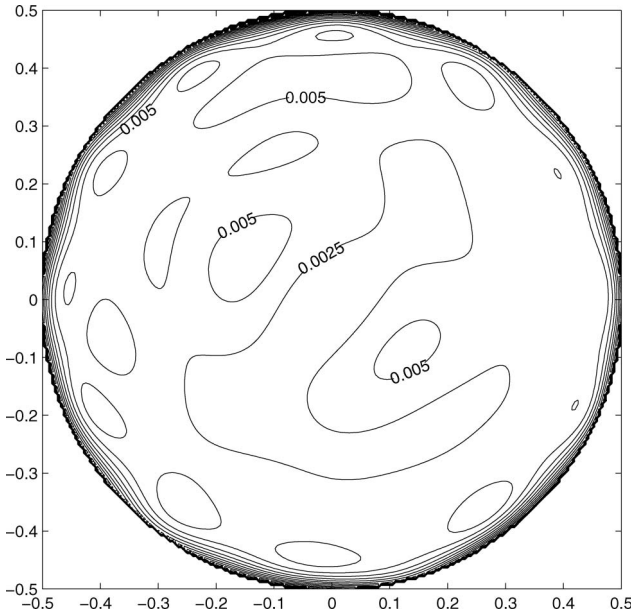

Fig. 4. Wavefront variance for a 6 mm pupil calculated using 20,000 eyes simulated according to the Thibos model with the first 15 Zernike modes removed. The units are micrometers squared.

- a 35-channel bimorph deformable mirror from AOptix (AOptix35) [46],
- a 52-channel magnetic deformable mirror from Imagine Eyes (MIRAO52), and
- a 140-channel MEMS device from Boston Micromachines (BMC140) [47].

The characteristics of these mirrors are presented in Table 1 and the differences in the actuator layouts will be discussed in Sections 4.A and 5.A (they will be shown in Fig. 7). More information on the mirrors can be found in the references given above.

In this paper, the performance of the mirrors has been determined by least-square fitting to wavefronts simulated to have aberrations with statistics corresponding to either the Kolmogorov model of atmospheric turbulence or the Thibos model of ocular aberrations. The method has been described elsewhere [26] and we will only summarize the important points here. The fitting performance requires determining the mirror modes and these were determined from laboratory measurements of the actuator influence functions. The measurements for all mirrors, except the segmented mirror, were obtained using a FISBA interferometer, which is a commercial Twyman–Green system. The segmented mirror was tested using a Zygo white-light interferometer. Using the singular value decomposition of the influence function matrix $\mathbf{M} = \mathbf{U}\mathbf{W}\mathbf{V}^T$, the projected wavefront, corresponding to the input wavefront Φ, can be written as the vector

$$\Phi_{\mathbf{M}} = \mathbf{U}\mathbf{W}\mathbf{V}^T f(\mathbf{V}\mathbf{W}^{-1}\mathbf{U}^T\Phi), \tag{5}$$

where $\mathbf{U}$ and $\mathbf{V}$ contain the orthogonal set of mirror modes in the phase and command spaces, respectively, and $\mathbf{W}$ represents the singular values. $\mathbf{W}$ can be truncated to a given number of modes N. f is the clipping function applied to the command vector $\mathbf{x} = \mathbf{V}\mathbf{W}^{-1}\mathbf{U}^T\Phi$ and defined by

$$f(x_i) = \begin{cases} x_i & \text{if } -x_{\text{lim}} \le x_i \le x_{\text{lim}} \\ x_{\text{lim}} \times \frac{x_i}{|x_i|} & \text{if } x_i < -x_{\text{lim}} \quad \text{or} \quad x_i > x_{\text{lim}} \end{cases}. \tag{6}$$

For each mirror, we independently varied the size of the correction aperture on the mirror and the number of modes used for correction in order to find the optimal parameters for the best average achievable correction for the set of aberrations considered. The spatial characteristics of the residuals were analyzed so as to determine the limiting factors. The results are given in the next section.

Table 1. Characteristics of the Deformable Mirrors Studied

Mirror	Optical Diameter (mm)	Individual Stroke (μm)	Total Stroke (μm)
OKO37	15	0.3–0.6	3.5
AgilOptics37	16	0.2–0.6	3
IrisAO37	3.5	5	4.3
OKO19_PZT	30	3, 7–9	-
OKO37_PZT	30	2, 3.5–5	-
AOptix35	10.2	3, 7	16
MIRAO52	15	10–15	25
BMC140	3.3 × 3.3	1.5	3.5

4. Mirror Performance for the Correction of Ocular Aberrations

Using the statistical model given by Thibos *et al.* [42], we generated 100 typical ocular wavefronts for a 6 mm diameter pupil. Piston, tip, and tilt were removed from the Zernike decomposition, since these are usually ignored or precorrected in ocular AO systems. The initial wavefront error rms was calculated for each generated ocular wavefront as the norm of the Zernike coefficients, $\text{rms} = (\Sigma_i Z_i^2)^{1/2}$, according to the decomposition given in Eq. (1). The average wavefront error rms across the population was 0.68 μm. The best fit that could be obtained from each mirror was calculated for each ocular wavefront according to Eq. (5). The residual wavefront error was defined as $\Phi - \Phi_{\mathbf{M}}$ and the residual wavefront error rms calculated from all the j wavefront points as

$$\text{rms} = \sqrt{\frac{1}{N_j}\sum_j (\Phi(j) - \Phi_{\mathbf{M}}(j))^2}, \tag{7}$$

with N_j the number of phase points in the pupil.

A. Optimization of the Number of Modes and Optical Pupil

As mentioned earlier, the correction of ocular aberrations was optimized by adjusting the number of modes used for correction, as well as the size of the optical pupil for each mirror. Figure 5 shows an example of this study for the mirror OKO19_PZT.

The three curves correspond to the average wavefront error rms, after fitting the ocular wavefronts with the mirror, as a function of aperture ratio (the portion of the mirror diameter used for correction), for three different truncations of the **W** matrix. As can be seen in Fig. 5, the residual wavefront error rms first decreases as the aperture ratio is decreased and then increases again after reaching a minimum. The optimum number of modes used for correction depends on the aperture ratio and an optimum combination of correction aperture and number of correction modes can be found. The minimum average rms wavefront error is obtained for 64% of the mirror diameter and 17 modes. More insight into the effect of the aperture ratio can be gained with a spatial analysis of the wavefront error residual. Figure 6 shows the wavefront maps after correction of a typical ocular wavefront, with the full mirror diameter and the optimized pupil diameter, and the associated projections of the apertures on the actuator layout. For the full mirror diameter, it can be seen that the residual is more pronounced at the edges, showing a need for larger correction amplitude in this area. The residual wavefront error is more uniform for the optimized pupil when there is a ring of actuators outside the correction pupil: the calculated rms is 0.11 μm in the optimized case, as compared to 0.17 μm in the nonoptimized case.

A similar behavior was observed for the OKO37_PZT; a reduction of the optical pupil resulted in a significant improvement of the wavefront error residual, with the rms residual wavefront error dropping from 0.09 μm to 0.05 μm when averaged over all the ocular wavefronts. As regards the other mirrors, we can single out the membrane mirrors, such as the OKO37 and the AgilOptics37. It has been noted several times in the literature [17,26,48,49] that, since the membranes are fixed around their perimeter, it is necessary to use an optical beam smaller that the mirror diameter to control the wavefront at its edge.

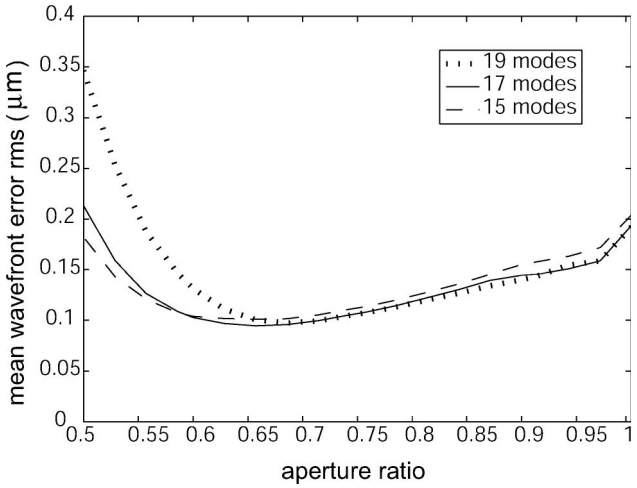

Fig. 5. Performance of the OKO19_PZT as a function of mirror aperture ratio, for 19, 17, and 15 modes used in the fitting expression.

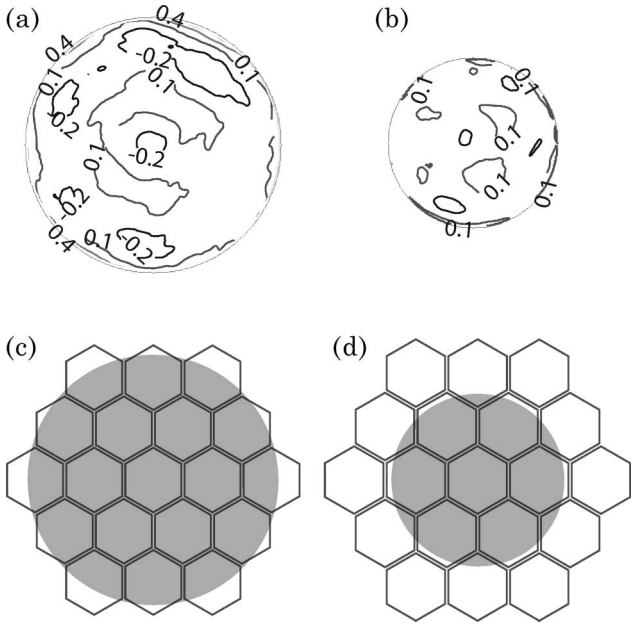

Fig. 6. Residual wavefront maps after correction of a typical ocular wavefront with the OKO19PZT: (a) using the full mirror aperture, (b) using half the diameter (units in micrometers); and projections of the pupils on the actuator layout: (c) full pupil, (d) optimized pupil.

For these three mirrors, we found an optimized optical pupil equal to about 60% of the full area covered by the actuators. Because of saturation, it was also necessary to reduce the number of modes used for correction to get the optimal fitting. As for the AOptix35 and the MIRAO52, the optical pupil set by the manufacturers proved to be approximately optimized and the full number of modes could be used. Finally, neither of these two parameters affects the IrisAO37, for which the control is zonal. The optimized optical pupils are shown superimposed on the actuator layout for all mirrors in Fig. 7 and the optimum parameters (number of modes and optical pupil) are given in Table 2. A decrease in the optimum number of modes reflects stroke limitation, particularly evident for the membrane mirrors, OKO37 and AgilOptics37.

B. Performance Comparison Among Mirrors

The performance of all the mirrors is presented in Fig. 8(a) in terms of mean wavefront error rms after fitting of ocular wavefronts. The numbers given are the best means of the residual wavefront error rms values. The optimized parameters (number of modes and aperture ratio) were found globally for all ocular wavefronts; perhaps a better optimization could be obtained for each individual ocular wavefront, resulting in an overall lower mean rms, but this was not the purpose of the study. We also show the corresponding average Strehl ratios in Fig. 8(b). These were calculated as the peak value of the oversampled point-spread functions reconstructed from the wavefront errors divided by the peak value of the diffraction-limited point-spread function,

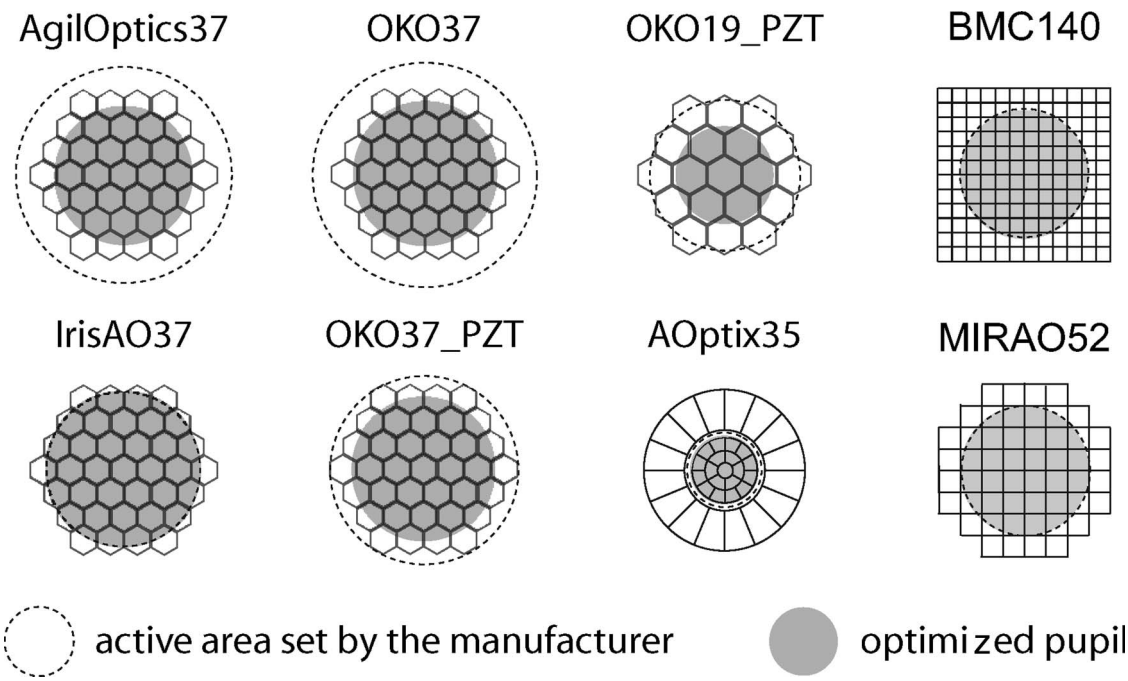

Fig. 7. Initial and optimized optical pupil superimposed on the actuator layout.

according to the definition of Strehl ratio of Born and Wolf [33]. This ignores any residual shift of the image, which we assume can be corrected in postprocessing, if necessary. The point-spread functions are calculated for a wavelength of 600 nm; we do not use polychromatic point-spread functions as in AO-assisted retinal imaging, the illumination sources normally have a narrow passband. The two figures give a ranking of the mirrors for the static compensation of typical ocular aberrations following an ophthalmic precorrection. The two similar membrane mirrors, the AgilOptics37 and the OKO37, yield poor performance for typical 6 mm ocular wavefronts. This is mainly due to their limited stroke, as we will discuss below. Interestingly, the IrisAO37, the BMC140, and the OKO19_PZT show comparable performance, although they have very different characteristics. All three give a mean wavefront error residual rms of less than 0.1 μm, although the Strehl ratios evidence some difference in performance. Finally, the MIRAO52, the AOptix35, and the OKO37_PZT can achieve diffraction-limited performance (Strehl ratio over 0.8), according to the simulations.

Table 2. Optimum Aperture and Number of Modes for Each Mirror

Mirror	Optimum Aperture (ratio of the full mirror diameter)	Optimum Number of Modes
AgilOptics37	62%	11
OKO37	63%	14
OKO19_PZT	64%	17
BMC140	100%	100
IrisAO	100%	37
OKO37_PZT	76%	34
AOptix35	89%	35
MIRAO52	100%	52

C. Spatial Analysis of the Wavefront Residuals

Figure 9 shows an example of the residuals for ocular wavefront correction by the different deformable mirrors; one can appreciate the very different patterns of wavefront errors produced by the mirrors. For most of the mirrors, we decomposed each simulated ocular wavefront error residual into Zernike polynomials up to 7th order, and calculated the norm N_r for each Zernike radial order r as

$$N_r = \sqrt{\sum_m (a_r^m)^2}, \tag{8}$$

with m the azimuthal frequency index and a_k^m the Zernike polynomial coefficient according to the ANSI double-indexing convention [34]. This spatial frequency analysis was performed in order to provide insight into the spatial resolution and stroke limitations of the mirrors.

The average values over the 100 wavefronts are presented in Fig. 10. The calculations were not performed for the IrisAO37 mirror, which is segmented and, hence, cannot be directly compared to the continuous mirrors in terms of spatial-frequency content. For most mirrors, the average difference between the rms given by the Zernike decomposition and the total rms of the wavefront (see Eq. (4)) was around 0.02–0.03 μm. The discrepancy was 0.06 μm for the BMC140; this higher value is probably due to the fine structure of the mirror, visible in Fig. 9. Here are the main points that can be made:

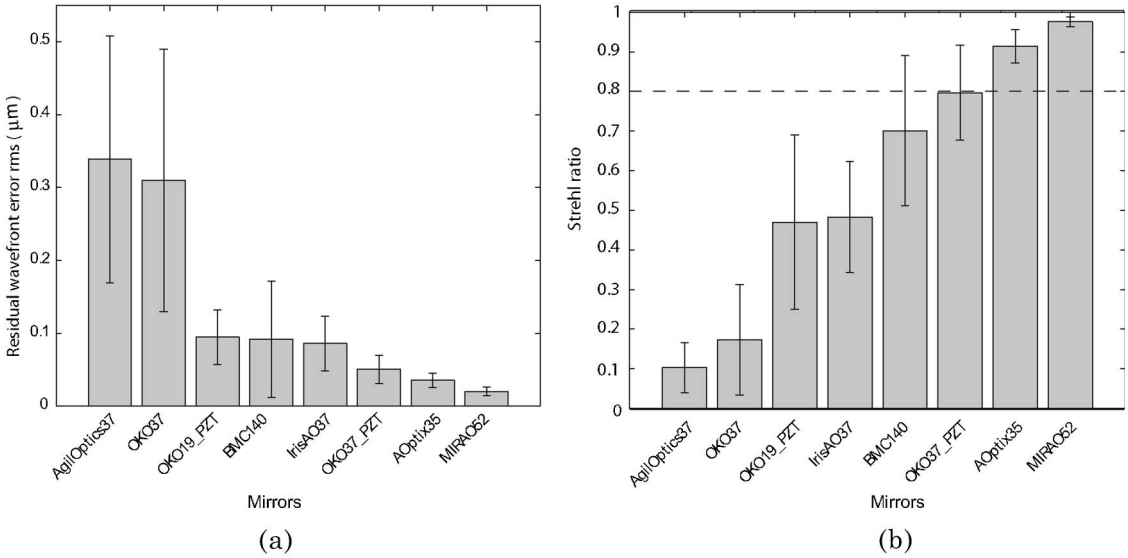

Fig. 8. Performance of the mirrors in correcting ocular aberrations. (a) Mean residual wavefront error rms after the best fit given by the mirrors. (b) Mean Strehl ratio after the best fit given by the mirrors. The error bars represent ±1 standard deviation.

- An important parameter highlighted by this mirror comparison is the required stroke; in particular, the OKO37 and the AgilOptics37, which have the same characteristics, have at least one actuator clipping for 97% and 98% of the ocular wavefronts, respectively, with the optimized parameters. For these two mirrors, the saturation is visible in the wavefront residuals in Fig. 9, and results in the high values of the norm for low Zernike radial orders, in particular, for orders 2, 3, and 4. The BMC140 also saturates for 80% of the eyes. Although it is less pronounced, it can be seen, especially in Fig. 10(b), that the low-order mode residual is more important than the high-order mode residual.
- The stroke is not an issue for the OKO19_PZT, but the structured residual wavefront plots, as well as the corresponding Zernike decomposition in Fig. 10, indicate that its performance is limited by the number of actuators. Indeed, the Zernike norm can be seen to increase rapidly from the 4th order.
- Although they have very similar characteristics in terms of number of actuators and stroke (see Table 1), the OKO37_PZT and the AOptix35 do not have the same residual error. When simulating the performance of the OKO37_PZT with a stroke equivalent to that of the AOptix35 (1.5 times its current stroke), we found that the former did not quite catch up with the latter. The slight remaining difference may be attributed to the arrangement of actuators possibly more suited for ocular aberrations in the case of the AOptix35, or else to the shape of the influence functions. In Fig. 10(b) the residual can be seen to increase with the Zernike order for these two mirrors, indicating that they are limited by their spatial resolution.
- The MIRAO52 appears to be the best mirror for the correction of ocular aberrations. It exhibits enough stroke and a good layout of actuators as set by the manufacturer; the Zernike norm of the residual wavefronts is much flatter throughout the Zernike orders.

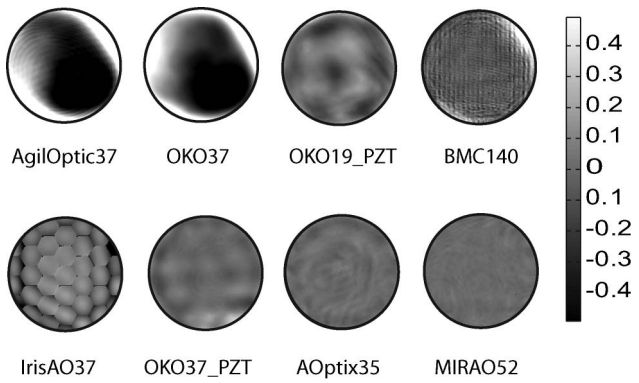

Fig. 9. Wavefront residuals after fitting of a typical ocular wavefront with the deformable mirrors (scale in micrometers).

D. Discussion

Our results can be compared to previous studies reported in the literature. Kennedy and Paterson [49] simulated the performance of two of our mirrors, using the same ocular wavefront model. They did not use direct measurements of the influence functions, but rather determined them from finite-element modeling. The results are not directly comparable, however, since they removed the second-order terms before performing the fitting. We carried out the calculations in similar conditions and found, for the OKO37, a Strehl ratio of 0.11 calculated with the expression they use for a 6 mm ocular pupil; the value fits with the contour plot they give for this mirror. As for the BMC140, we get a Strehl ratio of 0.9 when removing defocus and astigmatism from the ocular wavefronts. Our mirror has a total stroke of 3.5 μm; hence, the result compares well to their simulations indicating a Strehl ratio of 0.7 for a mirror with a stroke of 2 μm, and a Strehl ratio

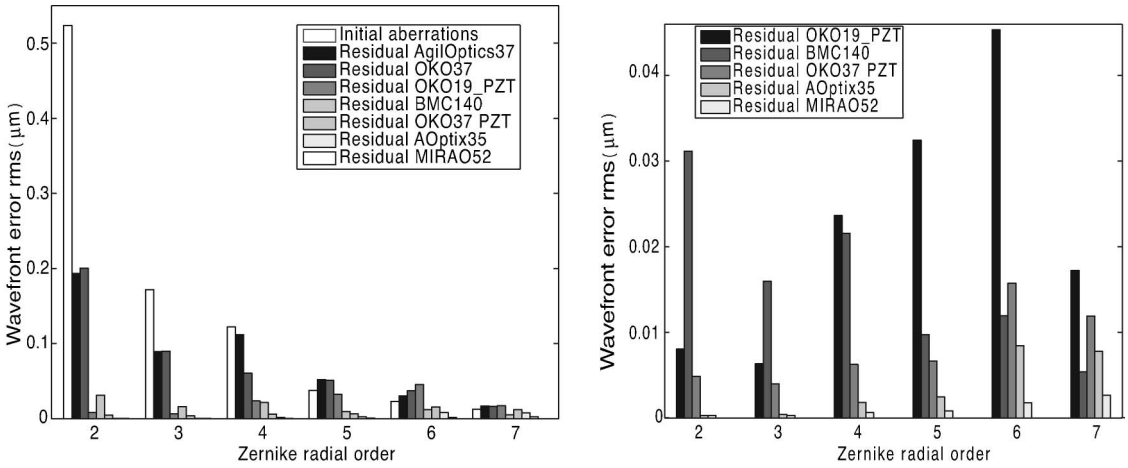

Fig. 10. Mean rms of the ocular wavefront residuals for each Zernike radial order: (a) initial and residual wavefronts after correction with all mirrors, (b) zoom on the residual of the five best mirrors.

slightly higher than 0.9 for a mirror with twice the stroke. In another paper, Bonora and Poletto [50] presented the performance of a new push–pull membrane mirror and compared it to the pull-only version of the mirror, similar to our OKO37. They simulated the performance of the mirrors by fitting 100 aberrated eyes following the statistics published by Castejón-Mochón *et al.* [40] and found a residual rms wavefront error $\sigma = 0.3\,\mu$m for the pull-only membrane mirror, in good agreement with the results we presented. The value was reduced to $0.1\,\mu$m with the push–pull mirror, demonstrating the gain in performance that can be obtained with a higher stroke.

We pointed out in our analysis that stroke-limited mirrors exhibit high residuals in the low-order modes, while the spatial-resolution-limited mirrors have a residual that increases with the radial order. This observation agrees well with the analysis of the statistics of ocular aberrations given in Subsection 2.B: the wavefront variance is the highest for low-order modes and decreases rapidly with the radial order. Therefore, most of the stroke is dedicated to the correction of low-order modes and they will be the most affected by a limitation in the mirror stroke. The other implication is that a high number of modes, hence actuators, is not necessary for a good correction of ocular aberrations. In fact, our simulations show that 35 are sufficient, since both the AOptix35 and the OKO37_PZT achieve diffraction-limited correction. This result may appear contradictory to the predictions given by Doble *et al.* [51]. Applying their model to the Thibos 6 mm ocular wavefronts, they get a resulting Strehl ratio of 0.5 for a discrete actuator deformable mirror with seven actuators across, like the OKO37_PZT analyzed here. The discrepancy can be explained by the optimization of the optical pupil, which, as mentioned earlier, significantly improved the mirror performance. Our results showing the need for an outer ring of actuators agree well with the study by Vdovin *et al.* [52] on the correction of low-order aberrations with continuous mirrors. They derive equations for the number of actuators required outside the working aperture for each type of mirror (membrane, bimorph, and continuous facesheet mirrors) as a function of Zernike order. The equations cannot be directly applied to our case, since ocular aberrations are a combination of Zernike polynomials. However, they show the requirement for all continuous mirrors to have some actuators placed outside the edge. Typically, we found that, when stroke is not an issue, a ring of actuators should be placed outside the pupil for ocular aberrations. This geometry fits the statistics of ocular aberrations, which, as we have seen, show higher variance at the edges of the pupil.

5. Atmospheric Wavefront Correction

We have seen that wavefront aberrations caused by passing through atmospheric turbulence differ statistically from ocular aberrations, tending to have relatively larger high spatial frequency content (Fig. 1). It can be expected that the performance of the deformable mirrors presented in the Section 4 will be different when correcting wavefronts aberrated by passing through atmospheric turbulence, and we have examined this by least-squares fitting of the mirrors to phase screens simulated to have Kolmogorov statistics. The phase screens were generated using an algorithm described by Harding *et al.* [53]. It involves simulating low resolution screens by factorization of the theoretical Kolmogorov covariance and interpolation to produce screens of the required size. The screens were simulated with $D/r_0 = 7.5$, which, with piston and tip–tilt removed, will give an rms wavefront error equal to that of the Thibos model for a 6 mm eye. In the case of observing through turbulence, it corresponds to either a small aperture at visible wavelengths or a modest aperture at infrared wavelengths, but is appropriate for low-cost AO systems. The outer scale of the simulated

turbulence is infinite, i.e., it is pure Kolmogorov turbulence. The average root-mean-square wavefront error for 100 simulated screens was found to be 0.69 μm.

A. Optimization of the Number of Modes and Optical Pupil

For every wavefront to be corrected by a DM there is an optimum number of mirror modes and pupil diameter which depends on the spatial profile of the wavefront and the spatial response of the mirror. While reducing mirror modes and aperture diameter limits the spatial resolution of a correcting device, it does increase fitting performance to lower-order aberrations. The effect of these parameters on the OKO19 DM can be seen in Fig. 11. In this case there is less variability in performance compared to the ocular wavefront case. While the variance of the wavefront with piston–tip–tilt corrected is higher at the edge of the aperture, it is found that reducing the optical pupil with respect to the deformable mirror actuated aperture only leads to a slight increase in performance. The optimal ratio of optical to actuated aperture is 0.88.

B. Performance Comparison Among Mirrors

The fitting performance for each mirror, characterized by the residual wavefront error rms and Strehl ratio at 2.2 μm, is given in Fig. 12, along with the standard deviation of the 100 samples. This wavelength was chosen as the center of the atmospheric K band, which is the most likely observation wavelength for AO on a moderate (~4 m) aperture telescope with the relatively low-order mirrors considered here. The Strehl ratio is calculated using the peak of the point-spread function intensity for the residual wavefronts. The AgilOptics mirror and the OKO37 do not have the required stroke or actuator density to adequately correct wavefronts for this level of turbulence. The mirrors with large amounts of stroke performed much better with differences between the AOptix35, OKO37 PZT, and the MIRAO52 largely due to actuator arrangement and influence function shape. The MIRAO52 in this case lacked the spatial resolution of the BMC140, but its large stroke made it the most uniform across the radial orders of all the devices. The BMC140 achieved the highest Strehl ratio of 0.72.

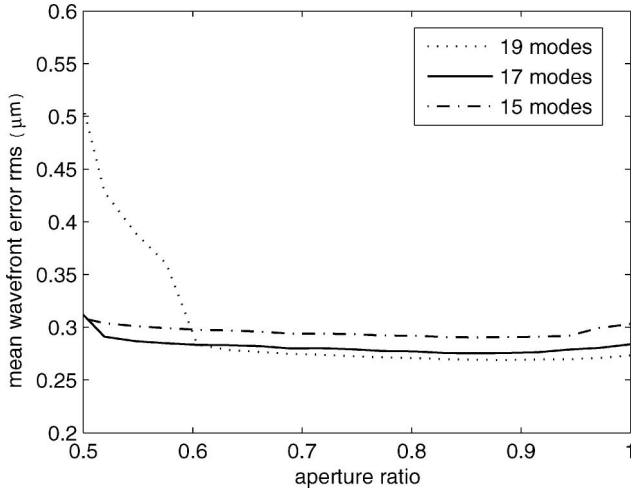

Fig. 11. Performance of the OKO19_PZT as a function of mirror aperture ratio, using 19, 17, and 15 modes to fit to wavefronts simulated to have Kolmogorov statistics with $D/r_0 = 7.5$.

None of the mirrors achieved Strehl ratios higher than 0.8. Such performance would only be achieved on a real telescope with smaller D/r_0 or in a system using two deformable mirrors in a woofer–tweeter configuration [54].

C. Spatial Analysis of the Wavefront Residuals

More information on the performance of each mirror can be obtained by decomposing the residual wavefronts into Zernike polynomials. In Fig. 13 the mean rms error for each Zernike radial order is presented. Extending the results up to the 13th radial order allows for the larger-amplitude high-frequency aberrations to be observed. Residual tip–tilt and piston modes are not included. The residual high-order aberrations are much higher than in the case of correcting ocular wavefronts, reflecting the greater content of high-order aberration in the atmospheric wavefronts. As before, the AgilOptics mirror and the OKO37 do not have sufficient actuator stroke to give good correction. For this reason, the number of modes had to be reduced from 37 to 7 and 11, respectively, which has impacted on the higher spatial-frequency correction. The OKO_19PZT mirror performs very well in the lower frequency range, with correction falling off after the 4th radial order. The 37 actuator version of this mirror builds on this with the larger number of actuators accounting for a Strehl ratio of 0.64. Despite having relatively low stroke, the 140 actuator BMC140 mirror performed the best of all, achieving a balance between low- and high-order correction.

6. Conclusions

We have compared the spatial statistics of wavefronts aberrated according to Kolmogorov statistics, as appropriate to imaging through turbulence, and according to the Thibos model, which is based on measurements of a sample of healthy eyes. The ocular wavefronts have nonzero mean and the wavefront variance is several times higher at the pupil edge than at the center. Turbulence-aberrated wavefronts have zero mean and slightly higher variance at the pupil edge (when at least one mode is removed). When decomposed onto Zernike polynomials, the ocular wavefronts have lower contributions from high-order Zernikes, but this contribution increases with pupil size.

We compared eight different deformable mirrors for the tasks of correcting ocular and atmospherically aberrated wavefronts. The mirrors are all commercially available and cover a range of actuator types and geometries. The performance of the mirrors

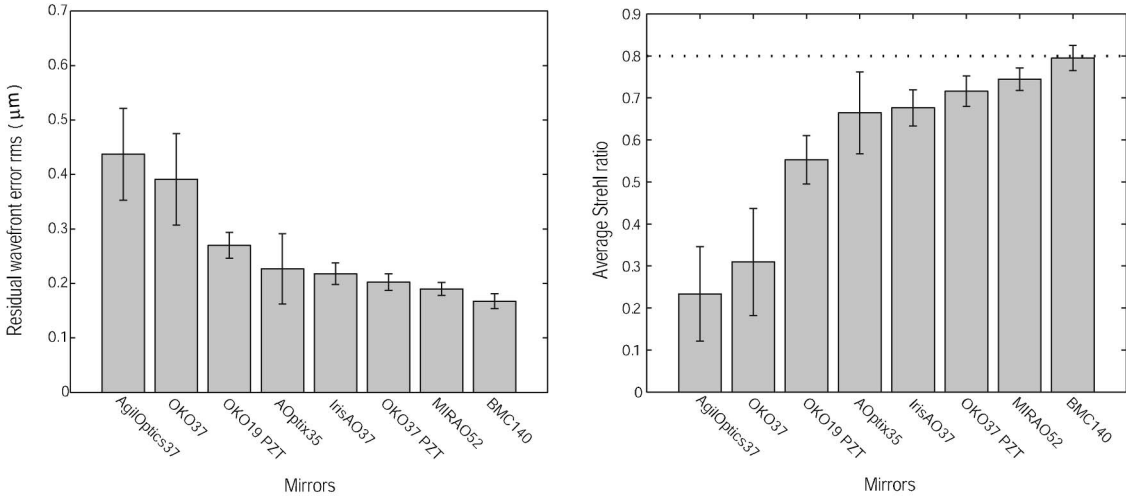

Fig. 12. Performance of the mirrors in correcting atmospheric aberrations. (a) Mean residual wavefront error rms after the best fit given by the mirrors, (b) Mean Strehl ratio at $\lambda = 2.2\,\mu$m after the best fit given by the mirrors. The error bars represent ± 1 standard deviation.

when correcting ocular wavefronts was found to depend critically on the size of the optical pupil relative to the actuator layout; for all mirrors except the segmented mirror, the correction is optimal when there is a ring of actuators outside the optical pupil, as this helps the correction of the pupil edge. It is found that a relatively low number of actuators can give high Strehl ratio, as the higher-order aberrations are less important. Stroke is a limiting factor in some cases, especially for the membrane mirrors, and it is manifested by low-order Zernike terms in the residual wavefronts. The best performance was obtained with the MIRAO52 magnetic mirror, and very good performance was also obtained with the AOptix35 bimorph mirror. These two mirrors combine high stroke and adequate number of actuators, as evidenced by the smooth residuals shown in Fig. 9.

In the case of correcting atmospheric wavefronts, it was found that there is a weak dependence of performance on the optical pupil size on the mirrors. For most mirrors, the performance is limited by the stroke or the low number of actuators. The residual errors would be acceptable only in a system with small D/r_0. The best performance in that case was obtained with the BMC140 micromirror and, again, very good performance was obtained with the MIRAO52 magnetic mirror. Good performance was achieved in both cases with the 37 actuator piezoelectric mirror from OKO and the 37 element segmented mirror from IrisAO. Table 3 summarizes the performance for all mirrors in the cases of correcting ocular aberrations and atmospheric aberrations.

Finally, when discussing the fitting performance of the deformable mirrors, the initial deformation of the mirror should be taken into account, as this may further limit the stroke available for correcting wavefronts. The initial shape of the mirror can be measured by interferometry at the command midrange and tip, tilt, and defocus should be removed, as these aberrations would easily be independently corrected in an AO system. The resulting wavefront error can then be added to the ocular wavefronts to be fitted in the simulations. Such calculations showed that the bias had a very small effect on the MIRAO52 (the mean residual wavefront error

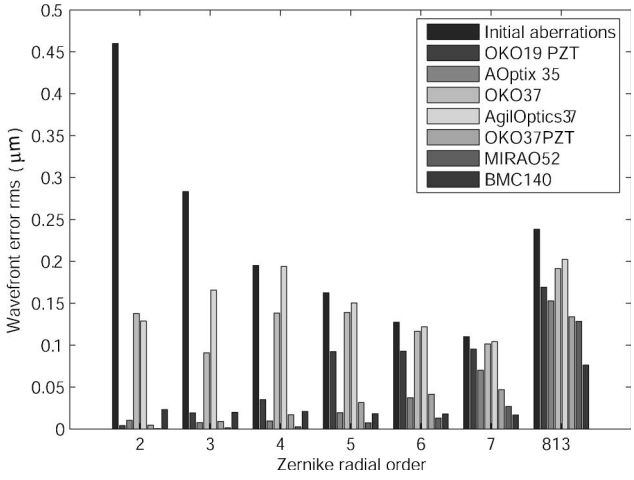

Fig. 13. Mean rms of the wavefront residuals for each Zernike radial order.

Table 3. Comparison of Residual Wavefront Error RMS for Atmospheric and Ocular Aberrations

	Residual rms (micrometers)	
Mirror	Atmospheric	Ocular
AgilOptics37	0.437	0.338
OKO37	0.391	0.310
OKO19_PZT	0.270	0.095
BMC140	0.167	0.092
IrisAO	0.218	0.086
OKO37_PZT	0.202	0.050
AOptix35	0.227	0.035
MIRAO52	0.190	0.020

rms increased to 0.027 microns), but the effect can be more important for other mirrors that have less stroke.

The measurements reported in this paper were based on a sample of mirrors purchased by our group; mirror performance will vary from mirror to mirror, and improvements in mirror performance by the manufacturers are ongoing. The study did not include a comparison of the temporal performance of the mirrors.

We would like to thank the manufacturers of the deformable mirrors used in this study for their assistance. In particular, we would like to thank AgilOptics, who provided the evaluation mirror used in this study and their technical team for support provided. This research is funded by Science Foundation Ireland under grant SFI/07/IN.1/1906.

References

1. H. Babcock, "The possibility of compensating astronomical seeing," Publ. Astron. Soc. Pac. **65**, 229–236 (1953).
2. V. P. Linnik, "On the possibility of reducting the influence of atmospheric seeing on the image quality of stars," original 1957 article translated and reprinted in *ESO Conference and Proceedings No. 48*, F. Merkle, ed. (Garching, 1993), pp. 535–537.
3. A. Buffington, F. S. Crawford, A. J. Muller, A. J. Schwemin, and R. G. Smits, "Active image restoration with a flexible mirror," Proc. SPIE **75**, 90–96 (1976).
4. J. Hardy, *Adaptive Optics for Astronomical Telescopes* (Oxford U. Press, 1998).
5. A. W. Dreher, J. F. Bille, and R. N. Weinreb, "Active optical depth resolution improvement of the laser tomographic scanner," Appl. Opt. **28**, 804–808 (1989).
6. H. Hofer, L. Chen, G. Y. Yoon, B. Singer, Y. Yamauchi, and D. R. Williams, "Improvement in retinal image quality with dynamic correction of the eye's aberrations," Opt. Express **8**, 631–643 (2001).
7. A. Roorda, F. Romero-Borja, W. J. Donnelly III, H. Queener, T. J. Herbert, and M. C. W. Campbell, "Adaptive optics scanning laser opthalmoscopy," Opt. Express **10**, 405–412 (2002).
8. A. Dubra, D. C. Gray, J. I. W. Morgan, and D. R. Williams, "MEMS in adaptive optics scanning laser opthalmoscopy: achievements and challenges," Proc. SPIE **6888**, 688803 (2008).
9. B. Hermann, E. J. Fernández, A. Unterhuber, H. Sattmann, A. F. Fercher, W. Drexler, P. M. Prieto, and P. Artal, "Adaptive optics ultrahigh resolution optical coherence tomography," Opt. Lett. **29**, 2142–2144 (2004).
10. J. W. Evans, R. J. Zawadzki, S. Jones, S. Olivier, and J. S. Werner, "Characterization of an AO-OCT system," in *Adaptive Optics for Industry and Medicine, Proceedings of the Sixth International Workshop, National University of Ireland, Galway*, C. Dainty, ed. (Imperial College Press, 2008).
11. G. Y. Yoon and D. R. Williams, "Visual performance after correcting the monochromatic and chromatic aberrations of the eye," J. Opt. Soc. Am. A **19**, 266–275 (2002).
12. E. J. Fernández, S. Manzanera, P. Piers, and P. Artal, "Adaptive optics visual simulator," J. Refract. Surg. **18**, S634–S638 (2002).
13. P. A. Piers, S. Manzanera, P. M. Prieto, N. Gorceix, and P. Artal, "Use of adaptive optics to determine the optimal ocular spherical aberration," J. Cataract Refract. Surg. **33**, 1721–1726 (2007).
14. K. M. Rocha, L. Vabre, F. Harms, N. Chateau, and R. R. Krueger, "Effects of Zernike wavefront aberrations on visual acuity measured using electromagnetic adaptive optics technology," J. Refract. Surg. **23**, 953–959 (2007).
15. E. Dalimier, C. Dainty, and J. L. Barbur, "Effects of higher-order aberrations on contrast acuity as a function of light level," J. Mod. Opt. **55**, 791–803 (2008).
16. J. Liang, D. R. Williams, and D. T. Miller, "Supernornal vision and high-resolution retinal imaging through adaptive optics," J. Opt. Soc. Am. A **14**, 2884–2892 (1997).
17. E. J. Fernández and P. Artal, "Membrane deformable mirror for adaptive optics: performance limits in visual optics," Opt. Express **11**, 1056–1069 (2003).
18. S. A. Cornelissen, P. A. Bierden, and T. G. Bifano, "A 4096 element continuous facesheet MEMS deformable mirror for high-contrast imaging," Proc. SPIE **6888**, 68880V (2008).
19. N. Doble, G. Yoon, L. Chen, P. Bierden, B. Singer, S. Olivier, and D. R. Williams, "Use of a microelectromechanical mirror for adaptive optics in the human eye," Opt. Lett. **27**, 1537–1539 (2002).
20. M. A. Helmbrecht, T. Juneau, M. Hart, and N. Doble, "Performance of a high-stroke, segmented MEMS deformable-mirror technology," Proc. SPIE **6113**, 61130L (2006).
21. M. Glanc, E. Gendron, F. Lacombe, D. Lafaille, J.-F. Le Gargasson, and P. Léna, "Towards wide-field retinal imaging with adaptive optics," Opt. Commun. **230**, 225–238 (2004).
22. E. J. Fernández, L. Vabre, B. Hermann, A. Unterhuber, B. Povazây, and W. Drexler, "Adaptive optics with a magnetic deformable mirror: application in the human eye," Opt. Express **14**, 8900–8916 (2006).
23. N. Devaney, D. Coburn, C. Coleman, J. C. Dainty, E. Dalimier, T. Farrell, D. Lara, D. Mackey, and R. Mackey, "Characterization of MEMs mirrors for use in atmospheric and ocular wavefront correction," Proc. SPIE **6888**, 688802 (2008).
24. T. Farrell, E. Daly, E. Dalimier, and C. Dainty, "Task-based assessment of deformable mirrors," Proc. SPIE **6467**, 64670F (2007).
25. E. Daly, E. Dalimier, and C. Dainty, "Requirements for MEMS Mirrors for Adaptive Optics in the Eye," Proc. SPIE **6113**, 611309 (2006).
26. E. Dalimier and C. Dainty, "Comparative analysis of deformable mirrors for ocular adaptive optics," Opt. Express **13**, 4275–4285 (2005).
27. A. V. Goncharov and C. Dainty, "Wide-field schematic eye models with gradient-index lens," J. Opt. Soc. Am. A **24**, 2157–2174 (2007).
28. J. A. Díaz, C. Pizarro, and J. Arasa, "A single dispersive GRIN profile for the aging human lens," J. Opt. Soc. Am. A **25**, 250–261 (2008).
29. F. Roddier, "The effects of atmospheric turbulence in optical astronomy," in *Progress in Optics* (North Holland, 1981), Vol 19, pp. 281–376.
30. D. L. Fried, "Optical resolution through a randomly inhomogeneous medium for very long and very short exposures," J. Opt. Soc. Am. **56**, 1372–1379 (1966).
31. F. Roddier, "The problematic of adaptive optics design," in *Adaptive Optics for Astronomy*, D. M. Allon and J.-M. Mariotti, eds., NATO ASI Series C: Mathematical and Physical Sciences (Springer, 1993), Vol 324, pp. 89–111.
32. R. J. Noll, "Zernike polynomials and atmospheric turbulence," J. Opt. Soc. Am. **66**, 207–211 (1976).
33. M. Born and E. Wolf, *Principles of Optics* (Cambridge U. Press, 1959).
34. American National Standards Institute (ANSI), "American National Standard for ophthalmics—methods for reporting optical aberrations of eyes," ANSI Z80.28 (ANSI, 2004).

35. J. Y. Wang and J. K. Markey, "Modal compensation of atmospheric turbulence phase distortion," J. Opt. Soc. Am. **68**, 77–87 (1978).
36. G.-M. Dai, "Modal compensation of atmospheric turbulence with the use of Zernike polynomials and Karhunen–Loève functions," J. Opt. Soc. Am. A **12**, 2182–2193 (1995).
37. R. Hudgin, "Wave-front compensation error due to finite corrector-element size," J. Opt. Soc. Am. **67**, 393–395 (1977).
38. R. Conan, "Mean-square residual error of a wavefront after propagation through atmospheric turbulence and after correction with Zernike polynomials," J. Opt. Soc. Am. A **25**, 526–536 (2008).
39. J. Porter, A. Guirao, I. G. Cox, and D. R. Williams, "Monochromatic aberrations of the human eye in a large population," J. Opt. Soc. Am. A **18**, 1793–1803 (2001).
40. J. F. Castejón-Mochón, N. López-Gil, A. Benito, and P. Artal, "Ocular wavefront aberration statistics in a normal young population," Vision Res. **42**, 1611–1617 (2002).
41. T. Nirmaier, G. Pudasaini, and J. Bille, "Very fast wave-front measurements at the human eye with a custom CMOS-based Hartmann–Shack sensor," Opt. Express **11**, 2704–2716 (2003).
42. L. N. Thibos, A. Bradley, and X. Hong, "A statistical model of the aberration structure of normal, well-corrected eyes," Ophthal. Physiol. Opt. **22**, 427–433 (2002).
43. D. T. Miller, L. N. Thibos, and X. Hong, "Requirements for segmented correctors for diffraction-limited performance in the human eye," Opt. Express **13**, 275–289 (2005).
44. M. P. Cagigal, V. F. Canales, J. F. Castejón-Mochón, P. M. Prieto, N. López-Gil, and P. Artal, "Statistical description of wavefront aberration in the human eye," Opt. Lett. **27**, 37–39 (2002).
45. G. Vdovin and P. M. Sarro, "Flexible mirror micromachined in silicon," Appl. Opt. **34**, 2968–2972 (1995).
46. D. A. Horsley, H. Park, S. P. Laut, and J. S. Werner, "Characterization for vision science applications of a bimorph deformable mirror using phase-shifting interferometry," Proc. SPIE **5688**, 133–144 (2005).
47. T. G. Bifano, J. Perreault, R. Krishnamoorthy Mali, and M. N. Horenstein, "Microelectromechanical deformable mirrors," IEEE J. Select Top. Quantum Electron. **5**, 83–89 (1999).
48. C. Paterson, I. Munro, and J. C. Dainty, "A low cost adaptive optics system using a membrane mirror," Opt. Express **6**, 175–185 (2000).
49. G. T. Kennedy and C. Paterson, "Correcting the ocular aberrations of a healthy adult population using microelectromechanical (mems) deformable mirrors," Opt. Commun. **271**, 278–284 (2007).
50. S.Bonora and L. Poletto, "Push—pull membrane mirrors for adaptive optics," Opt. Express **14**, 11935–11944 (2006).
51. N. Doble, D. T. Miller, G. Yoon, and D. R. Williams, "Requirements for discrete actuator and segmented wavefront correctors for aberration compensation in two large populations of human eyes," Appl. Opt. **46**, 4501–4514 (2007).
52. G. Vdovin, O. Soloviev, A. Samokhin, and M. Loktev, "Correction of low order aberrations using continuous deformable mirrors," Opt. Express **16**, 2859–2866 (2008).
53. C. M. Harding, R. A. Johnston, and R. Lane, "Fast simulation of a Kolmogorov phase screen," Appl. Opt. **38**, 2161–2170 (1999).
54. R. Conan, C. Bradley, P. Hampton, O. Keskin, A. Hilton, and C. Blain, "Distributed modal command for a two-deformable-mirror adaptive optics system," Appl. Opt. **46**, 4329–4340 (2007).